AIAA SciTech Forum
8-12 January 2024, Orlando, FL
AIAA SCITECH 2024 Forum

10.2514/6.2024-1136

Thrust Densification of Space Electric Propulsion Systems via Volumetrically Complex Materials

Graeme Sabiston*
University of California, Los Angeles, Los Angeles, CA, 90095, USA

Richard E. Wirz†‡
University of California, Los Angeles, Los Angeles, CA, 90095, USA
Oregon State University, Corvallis, OR, 97331, USA

Thrust densification of space electric propulsion (EP) technologies is necessary to enable future ambitious space missions and exploration, such as crewed missions to Mars. EP densification is primarily limited by the ability of thruster materials to withstand extreme plasma conditions. This research investigates the interconnected dynamics of maximizing current enhancement, the subsequent challenges of sputtering and arcing erosion, and the implications of a promising new class of advanced materials, Volumetrically Complex Materials (VCMs), for space electric propulsion systems. In comparison to standard materials, VCMs show enhanced ability to manage high levels of plasma energy and electrical current due largely to the combined advantages of principles such as geometric trapping and plasma infusion. The mechanisms of energy management and sputterant transport within VCMs are examined to gain insight into optimal VCM geometries, and the potential for leveraging advanced additive manufacturing methods is explored. VCM arcing response and favorable sublimation erosion characteristics are also determined via coupled computational and experimental analyses. The findings underscore the potential of VCMs to revolutionize material design for challenging plasma-facing applications germane to EP, paving the way for more durable and efficient propulsion systems.

I. Introduction and Background

A. AMPERE

The results presented in this work have been developed as a secondary, parallel effort to those completed in service of the U.S. Department of Energy's ARPA-E project, AMPERE: "*Advanced Materials for Plasma Exposed Robust Electrodes*" (Award No. DE-AR0001378). The goal of AMPERE is to research, develop, test, and deliver robust plasma-facing materials designed for fusion energy power plants. Many of the challenges the AMPERE project seeks to address have analogues in the realm of high-power density electric propulsion systems. As such, the insights and advancements made through the AMPERE initiative are expected to cross-fertilize and contribute significantly to the future of thrust-densification for electric propulsion technologies.

B. Thrust Densification

Achieving higher thrust and reducing system volume are key objectives in the development of future electric propulsion (EP) systems, and are vital for boosting spacecraft efficiency and expanding the range of achievable space missions. The high thrust density found in EP devices such as magnetoplasmadynamic (MPD) and arcjet thrusters is inextricably linked to the electrical current capacity of their electrodes [1]. The ability to efficiently conduct large amounts of current without compromising lifetime via cathode erosion has long been a challenge in designing these types of thrusters [2–6]. Cathode erosion occurs in these devices via two main mechanisms: sputtering, and sublimation erosion due to electrical arcs.

Sputtering, or the removal of material due to bombardment by energetic plasma species, is a ubiquitous phenomenon in EP devices, and occurs wherever there are plasma-facing materials [7–11]. Cathodes are particularly susceptible

*PhD Candidate, Mechanical and Aerospace Engineering, and graemes1@ucla.edu
†Adjunct Professor, Mechanical and Aerospace Engineering, wirz@ucla.edu
‡Boeing Professor, Executive Director of Aerospace Research Programs, richard.wirz@oregonstate.edu, AIAA Associate Fellow

to sputtering, as the large negative biases that are applied to them accelerate plasma ions to energies capable of high degrees of erosion. Increasing thrust density correlates to a higher flux of ions striking the cathode, exacerbating and accelerating sputtering erosion.

MPD and arcjet thrusters operate via arc plasma discharges, characterized by high plasma density and rapidly evolving, narrow conducting channels of electrical current. In order to reduce erosion involved with the rapid heating and subsequent sublimation that these cathodes invariably experience, many approaches have been attempted to utilize innovative new materials or cathode geometries. Even still, cathode erosion due to high power-density arcs is often reported as the leading life-limiting mechanism for these devices [12–15].

Thus, the development and characterization of advanced materials that are able to both process high electrical loads, and resist harsh plasma conditions are of vital importance in advancing the performance and longevity of space propulsion technologies.

C. Volumetrically Complex Materials

Volumetrically Complex Materials (VCMs) are an innovative category of materials distinguished by their special geometric properties, specifically their open-cell or porous configurations featuring interlinked ligaments (See Fig. 1). VCMs are specifically engineered to endure the dynamic interactions encountered by materials exposed to plasma. They can be produced through various methods, including chemical vapor deposition of metals like tungsten on pyrolytic carbon frameworks, or, more recently, through metal additive manufacturing (AM) techniques. The structure of VCMs may either be random, similar to a stochastic foam, or exhibit a highly structured, cage-like arrangement. VCMs' structural characteristics, such as the diameter of pores, and the sizes of the ligaments and surface featuring, can range from a few micrometers to several millimeters, depending on the intended plasma environment.

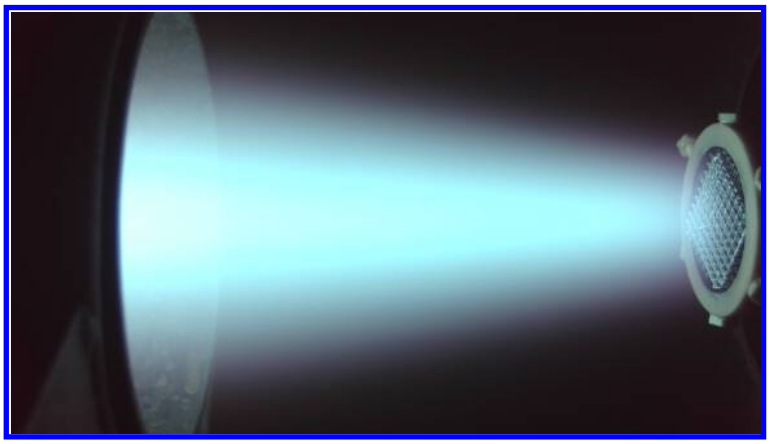

Fig. 1 Erosion of an additively manufactured volumetrically complex material (VCM), exposed to a magnetized plasma column.

Recent advances at the Plasma, Energy, and Space Propulsion Lab at UCLA have revealed that the unique geometric designs of VCMs contribute to their enhanced durability, especially when exposed to aggressive plasma environments, supported by various studies and publications [16–23]. Specifically, they have been shown to have a persistently reduced sputter yield, accomplished due to their ability to geometrically trap sputtered particles. The primary way that Volumetrically Complex Materials (VCMs) resist sputtering can be explained as follows: Even though the ligaments of a VCM exposed to plasma conditions undergo sputtering, most of the atoms dislodged from these ligaments are redeposited onto adjacent ligaments before they can leave the structure. Based on experimental evidence, it's believed that the "sticking coefficient" for sputtered particles is close to 100%, meaning that nearly all particles that interact with the ligaments are captured, and reintegrated back into the VCM structure [24, 25]. This presents a unique and exciting research opportunity in VCMs, given that the possibilities for geometric and material design in this domain are virtually limitless.

D. Objective and Organization

The objective of this study is to determine the opportunities for EP thrust densification that can be enabled by VCMs. Section II examines the current carrying behavior of VCMs through a canonical experiment to isolate and examine plasma infusion phenomena. Specifically, we aim to understand how their distinctive layered structure influences current distribution and assess their potential as high-power electrodes. We then turn our attention to the erosion mechanisms of sputtering and sublimation that accompany high current-carrying electrodes. In Section III, we go beyond examining the sputter yield of VCMs and focus on the specific mechanisms of sputterant transport to better understand these processes and inform more optimized designs. These sputtering experiments were completed with the first-ever additively manufactured VCMs for plasma-facing applications. Metal AM is a promising avenue to construct the unique geometries of optimized VCMs. However, the benefits and drawbacks of utilizing this advanced manufacturing method are remain largely unexplored. Therefore, this section will also address this knowledge gap and offer insight into the efficacy and potential challenges of AM VCMs. Finally, Section IV explores how VCMs react to high-power arcing conditions, delving into the physical and thermal dynamics of arcing on VCM structures via computational and experimental approaches.

This paper aims to explore these interconnected elements, providing a comprehensive background that spans the intricacies of current enhancement, the mechanisms and impacts of arcing and sputtering erosion, and the broader implications for EP system design. Through this exploration, we lay the groundwork for understanding and addressing the key challenges in the quest of thrust-densification of electric propulsion technologies.

II. Plasma Infusion and Current Carrying Capacity

For EP applications, the ability of VCMs to collect and efficiently transport high electrical currents is a critical attribute. In high-current applications, the high thermal loads due to the tens or thousands of amperes of current passing through the cathode can lead to rapid erosion and reduced lifetime. For example, VCMs can permit the infusion of plasma within the cathode structure, potentially allowing for a greater surface area from which electrons can be extracted into the plasma, when compared to conventional flat, unfeatured cathode surfaces.

A. Plasma Infusion

A key characteristic of evaluating the plasma material interactions for VCMs is the recently discovered metric of the plasma-infusion parameter, $\xi = \frac{D}{L_s}$, which is the ratio of the effective pore diameter of the VCM, D, and the local sheath length of the plasma, L_s. The plasma-infusion parameter also draws distinctions between VCM-plasma operating regimes of "plasma-facing" or "plasma-infused" [16]. The concept of plasma infusion is illustrated in Fig. 2, depicting a cross-section of a VCM and the varying depths of plasma penetration into the structure.

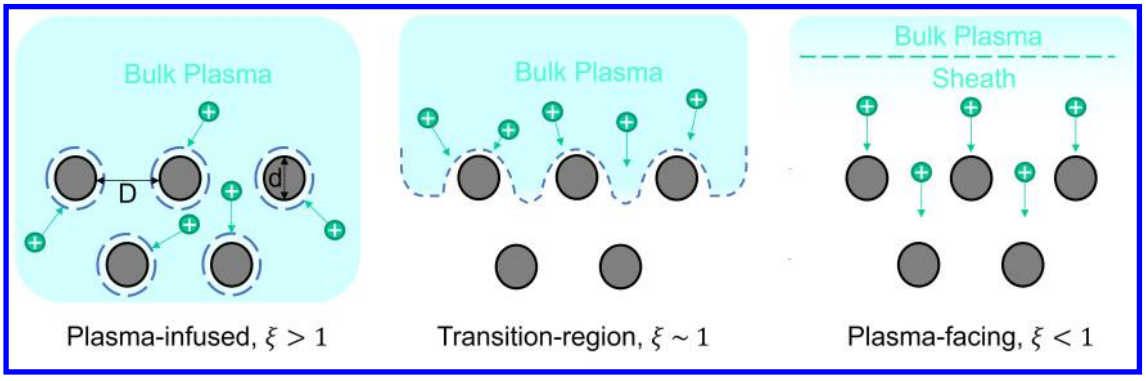

Fig. 2 Three regimes of plasma-material interactions - infused, transitional, and facing. The PMI regime is a function of the plasma properties of temperature and density, as well as the pore diameter of the VCM.

The formal construction of the plasma infusion parameter is as follows:

$$\lambda_D^2 = \frac{\varepsilon_0 k_B T_e}{n_e e^2} \tag{1}$$

$$\frac{L_s}{\lambda_D} = \frac{\sqrt{2}(2e\Delta\phi_s)^{3/4}}{3(k_B T_e)^{1/4}} \tag{2}$$

$$\xi = \frac{D}{L_s} \propto D\sqrt{n_e}(k_B T_e)^{1/4}\Delta\phi_s^{-3/4} \tag{3}$$

where λ_D is Debye length, ϵ_0 is the permittivity of free space, k_B is the Boltzmann constant, T_e is the electron temperature, n_e is the electron density, e is the fundamental charge, L_s is the Child-Langmuir sheath length, and ϕ_s is the applied bias to the VCM. The plasma-infusion parameter is therefore the ratio of the diameter of the open-cell VCM pores to the plasma sheath thickness. Based on this parameter, the PMI regimes can be classified into three categories: (1) plasma-infused regime ($\xi > 1$), (2) transitional regime ($\xi \approx 1$), and (3) plasma-facing regime ($\xi < 1$). Based on plasma infusion theory, the current-carrying behavior of VCMs is likely to vary significantly across different infusion regimes.

B. Surrogate VCM Experiment

To gain insight into the plasma infusion and current-carrying behavior of VCMs, we developed an experiment in which multiple, woven meshes are stacked upon one another, mimicking a VCM with a evenly-spaced layered configuration. The meshes consist of orthogonal circular strands, organized at regular intervals. The strands have diameters of 0.41 mm for the mesh with 0.86 mm pore size, and 0.64 mm for the mesh with 1.9 mm pore size. The entire mesh assembly is biased negatively with respect to the plasma potential to collect ion current, therefore acting as a cathode. The mesh assembly is then placed in a plasma column, and the current collected by each electrically

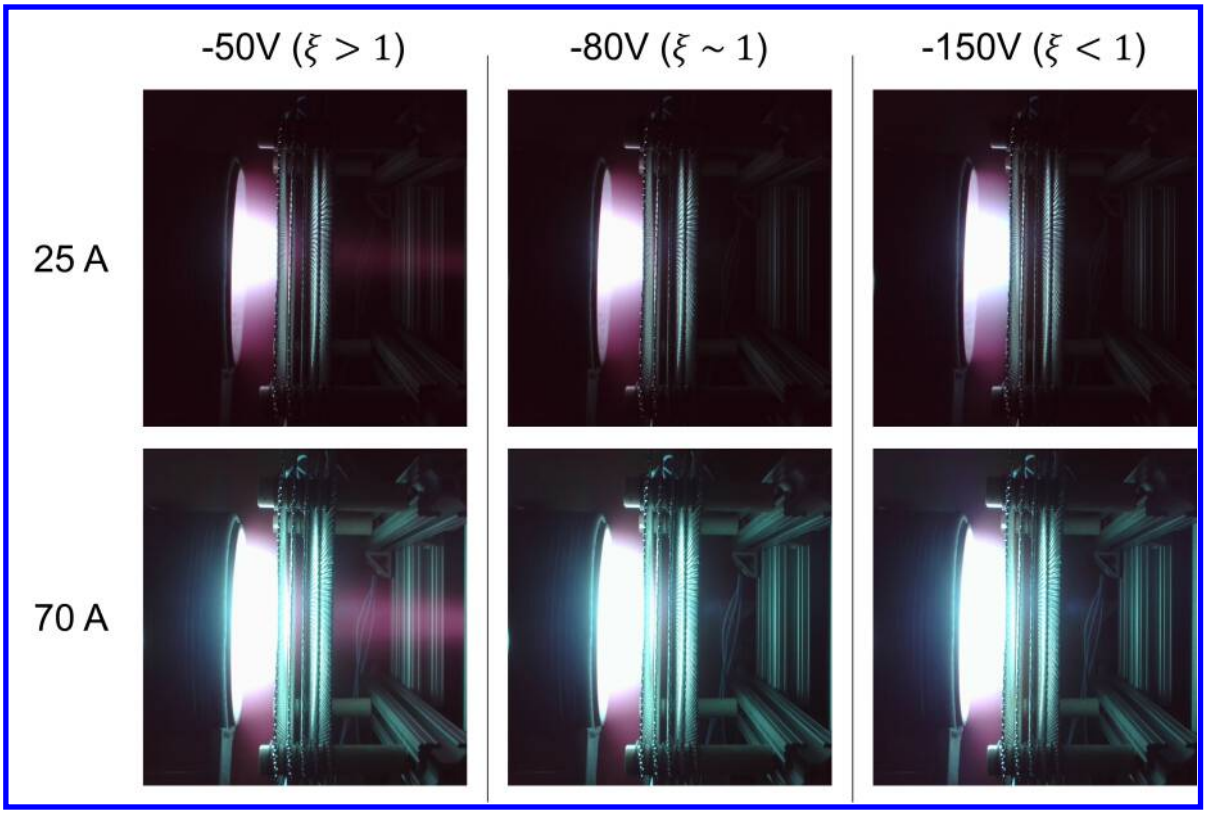

Fig. 3 Images of the surrogate VCM current carrying experiment at varying mesh biases and discharge currents. Five layers of steel meshes were stacked with equal spacing and biased to a negative potential, mimicking a layered VCM structure. The shift from plasma-infused to transitional can be seen by the lack of excited species beyond the last mesh, whereas the shift from transitional to fully plasma-facing is noted by the plasma column widening at the first mesh layer; this indicates a larger sheath forming, pushing the plasma column out radially.

isolated mesh layer is monitored via shunt resistors. By sweeping the electrical bias applied to the mesh assembly, the plasma infusion and consequent spread of total current distributed across the individual mesh layers can be assessed, and correlations between these characteristics can be made.

Fig. 3 depicts the surrogate mesh experiment at multiple applied biases and plasma discharge currents. The total current to the mesh assembly is fixed across all biases, with roughly 0.2 A and 0.45 A of current collected at 25 A and 70 A of plasma discharge current, respectively. At lower biases (floating to −80 V), the plasma is infused within the upper VCM layers. As the bias is increased, the total percentage of the current that is collected by the top-most mesh increases. This is predicted by infusion theory, as the sheath around the ligaments expands to collect a greater number of available ions, and therefore reduces the plasma density at lower layers of the VCM. A transitional regime, wherein the plasma-infusion parameter is on the order of unity, is reached between −80 V to −120 V, where the current to the top layer reaches a maximum. From −120 V onwards, the total percentage of current to the top layer starts to decrease as the mesh assembly enters a purely plasma-facing regime. The graph in Fig. 4 illustrates this correlation, showing the total percentage of the total current that is collected by the topmost mesh layer as a function of applied bias. In this regime of high applied bias, it is believed that the ions, gaining acceleration through the sheath now spanning millimeters from the mesh's upper surface, attain speeds that allow them to traverse the mesh pores. At this velocity, their trajectory is not significantly altered by attraction to the meshes, enabling them to continue ballistically to the lower mesh layers, which are at a uniform electrical potential.

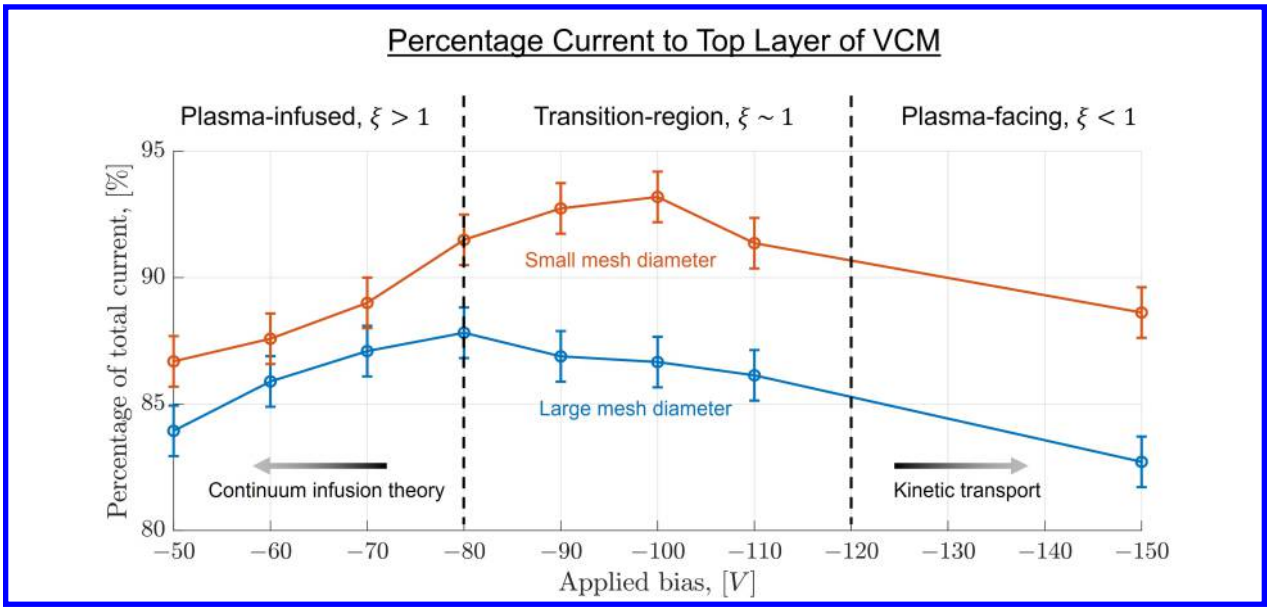

Fig. 4 Percentage of total current collected by the first layer of the stacked mesh structure as a function of applied bias, for two mesh pore sizes of 0.86 mm and 1.9 mm.

This finding has implications for VCMs as cathodes, as, when operated at sufficiently high biases to be in a plasma-facing regime, the total electrical load - and therefore, thermal load - may be spread more evenly across the VCM, as opposed to concentrating the collection of ions to the uppermost layers. Figure 5 shows this trade-off at higher biases, illustrating the distribution of total current across the top three layers of the mesh structure. The total current that is collected by the top layer decreases from 90% to 65% across an applied bias of −50 V to −400 V. This transition from "continuum infusion" to "kinetic transport" and the associated ion transport is to be explored further in a forthcoming computational manuscript.

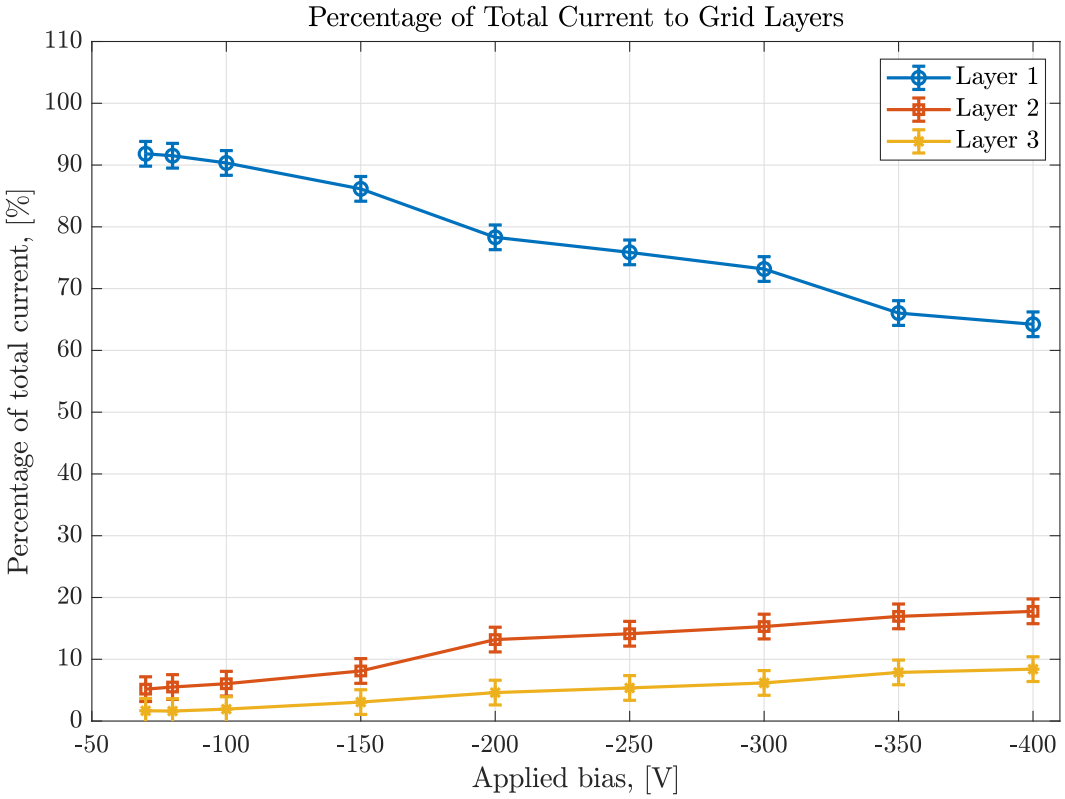

Fig. 5 Percentage of current collected by the top three layers of the stacked mesh assembly (25 A discharge current, 1.9 mm mesh pore size). As kinetic effects begin to dominate around -80 V onwards, the lower layers of the VCM collect a larger percentage of the total current.

III. VCM Sputtering Transport and Advanced Manufacturing

Recent research, including that by Li and Wirz [16], has highlighted the complexity of sputtering transport mechanisms in VCMs, especially in stochastic foam structures. These structures, due to their non-repetitive nature, exhibit varied sputtering and deposition rates across different ligaments, influenced by their unique angles of incidence with the plasma and the surrounding ligaments. This variability presents challenges in isolating specific transport mechanisms within VCMs. To address these challenges, metal additive manufacturing emerges as a promising method. By creating uniform, repeating ligament structures, this technique ensures that each part of the VCM experiences similar plasma sputtering conditions. This uniformity is expected to provide a clearer understanding of the sputtering mechanisms, as it reduces the confounding variables present in stochastic structures. However, the additive manufacturing process can also introduce non-idealities to the VCM geometry, such as voids and spatter. The effect of these features have yet to be fully understood in terms of their impact on sputtering and the evolution of the VCM structure. Therefore, this study aims to both provide insights into the sputtering processes and material deposition patterns, and also reveal how the characteristics inherent to AM VCMs influence their structural evolution.

Stainless Steel (grade 316L) was chosen as the material for additively manufactured VCMs two reasons. Firstly, 316L SS has a long history in the additive manufacturing industry, due to its exceptional “printability". Secondly, the sputter yield of 316L SS is relatively high, compared to refractory metals like tungsten that would be used in a real-world application of VCMs. A high sputter yield is favorable as it leads to shorter experiment times, with erosion and deposition processes occurring on more manageable timescales. The focus of this effort is to study uniform cage structures with triangular ligaments, creating a single preferred angle of incidence for incoming ions. The samples, pictured in Fig. 6, measure 1" in width and length, and 0.75" in height, with ligament sizes of 800 µm at the base of the triangles, and a pores-per-inch (PPI) count of 10 and 15. The VCM samples are placed into a vacuum chamber, and

exposed to plasma-facing conditions in a xenon plasma. The samples are electrically biased to −300 V, replicating 300 eV ions, and experience sputtering erosion for hours at a time. The samples are then removed, examined *ex-situ*, and placed back into the chamber for additional rounds of erosion.

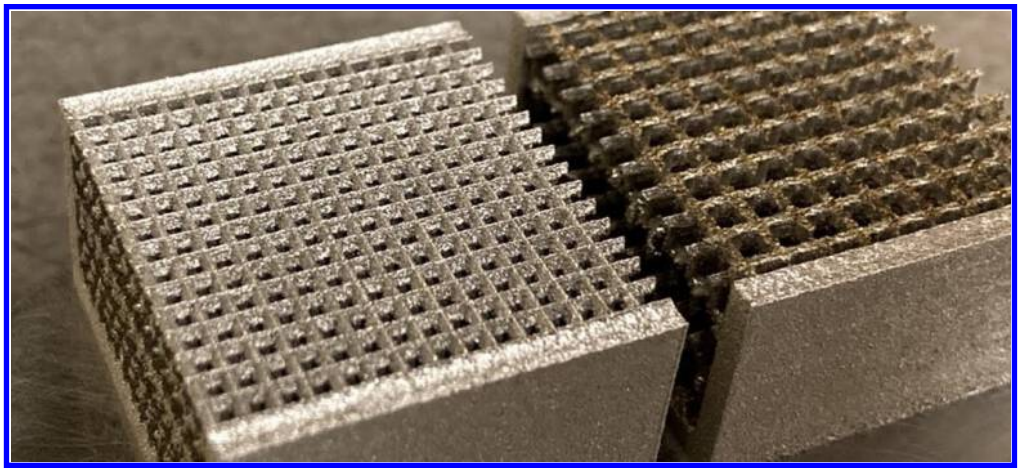

Fig. 6 15 PPI (left) and 10 PPI (right) 316L stainless steel VCMs, created via direct metal laser melting (DMLM) additive manufacturing.

A. Sputter Transport

Figure 7 depicts scanning electron microscope (SEM) images of the top-most ligaments of the 10 PPI VCM, after multiple rounds of plasma exposure. In this image, the VCM is viewed from the top surface, where the peak of the triangular ligaments are perpendicular to the incoming ions (i.e., the ions that are bombarding the VCM "see" the surfaces in Fig. 7 from their perspective). The ligaments erode due to sputtering, and project their sputtered material further down into the lower layers of the VCM, as well as some fraction that leaves the geometry completely, and contributes to the overall mass loss of the VCM. The erosion of the top-most ligaments can be quantified by noting that the ligament diameter decreases from 860 µm to 810 µm (−6% from original) after 6 hours, and then to 730 µm (−15% from original) after an additional 6 hours. Additionally, flat cylindrical features (Fig. 7 upper left, located between ligament vertices) that were implemented as control structures for normal incidence sputtering had almost completely been removed by 12 hours of erosion. This indicates that surfaces at normal incidence to the impinging plasma experience significant erosion if they do not receive adequate deposition from the surrounding geometry. Figure 8 shows the second layer of the 10 PPI VCM, and the accumulation of material deposited from sputtering of the top layer. The overall size of features increase on the order of 10 − 30%, depending on the initial feature shape and local surroundings. The size of these features can be anticipated to grow until the upper layers of the VCM erode sufficiently so as to allow a higher percentage of energetic plasma ions to bombard the surface. These images illustrates the concept of redeposition and geometric trapping of sputterants in VCMs, proving the validity of claims of sputter reduction.

B. Metal AM Considerations

As shown in the SEM images, prior to erosion, there exist many stochastic artifacts from the metal additive manufacturing process that comprise the surface structure of the ligaments. Spherical metal "spatter" balls are found on all surfaces, ranging from 10 µm to 100 µm. Additionally, the minimum track width of the DMLM process was on the order of 75 µm, shown by the top edge in the middle of the triangular ligament, in the bottom left image of Fig. 7; this parameter constrains the minimum feature size of the VCM. Note that these two consequences of the AM process lead to an "as-printed" geometry that departs from the initially designed part, which, in this case, was designed to have triangular ligaments with smooth faces, with a peak half-angle of 30° (i.e., an equilateral triangle). These small random features will initially break up the intended regularity of the structure, causing departures from predicted sputtering characteristics. However, as shown in the post-erosion images of Fig. 7, these surface features are gradually worn down to reveal an underlying structure that is more homogeneous. Additionally, the peak of the triangular ligament becomes sharp, in some places reaching only a few microns in size. Shown in Fig. 9, another key feature of AM VCMs is the

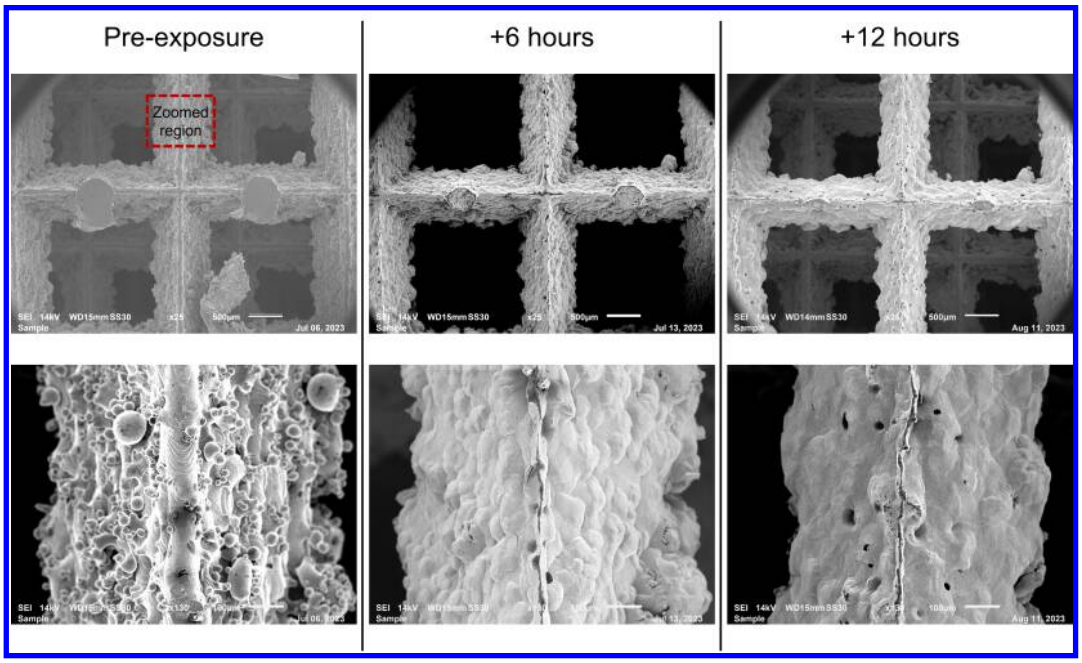

Fig. 7 Top-down view of the top layer of a 10 PPI, 316L stainless steel VCM, taken via scanning electron microscope. The upper row of images shows the same unit cell of the VCM, with increasing erosion from left to right. The bottom row depicts a magnified view of a single triangular ligament from the unit cell pictures above.

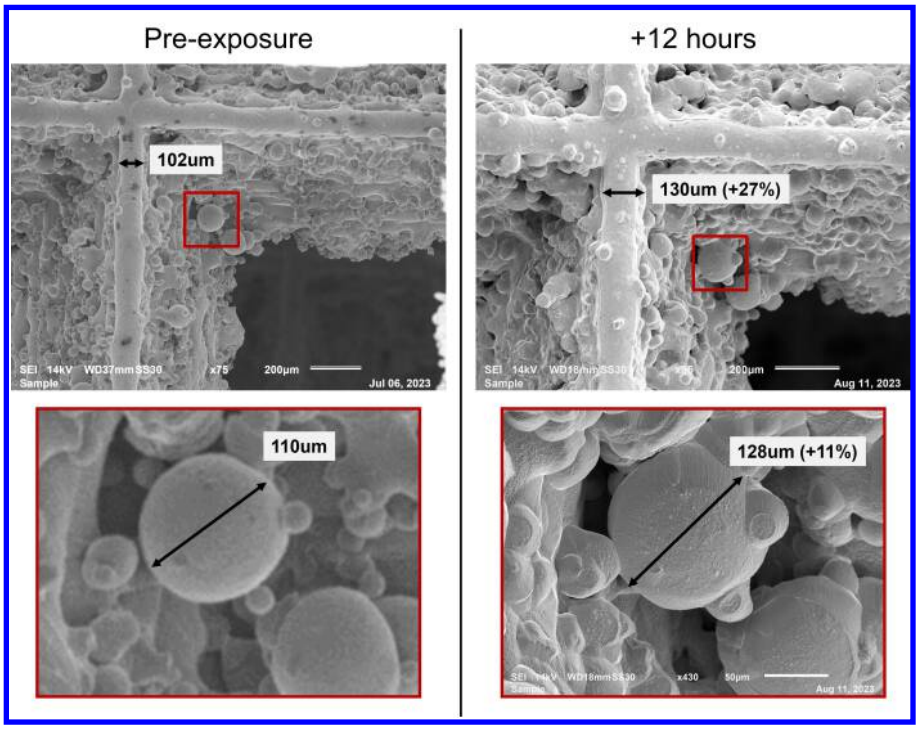

Fig. 8 Top-down view of the second layer of a 10PPI, 316L stainless steel VCM, taken via scanning electron microscope. This view looks through a pore of the top layers of the VCM to examine deposition of sputtered material from the top layer. Note that essentially all features experience some increase in size as they accumulate mass.

appearance of voids that can be seen in the 12 hour exposure tests. As the VCM receives sufficient fluence of ions, void regions where metal powder did not properly melt and integrate into the structure become visible and participate in sputtering process. While initially these may be seen as unwanted by-products of the AM process, these voids may aid in the geometric trapping of sputterants. As the void region is uncovered, its side walls may direct sputtered material down into the void, eventually filling and smoothing it. Therefore, the ligament material is retained in the upper layers of the VCM, instead of projecting it downwards into the structure - where it may not as efficiently be recycled later in the sputtering process - or out of the VCM entirely, thereby contributing to the global sputter yield of the VCM.

Additive manufacturing has thus proven to be a practical way to both create VCMs, and conduct controlled experiments on sputter transport processes. However, it is crucial to weigh the imperfections and artefacts of the AM process against the ease of manufacturing and the potential benefits it may offer in sputtering processes. Further research is necessary to examine the ability to control these process parameters to decrease the differences between the designed VCM and the printed VCM, as well as to determine if there are optimal geometries for minimizing sputtering that can leverage the inclusion of voids, or other AM-related features in the final design.

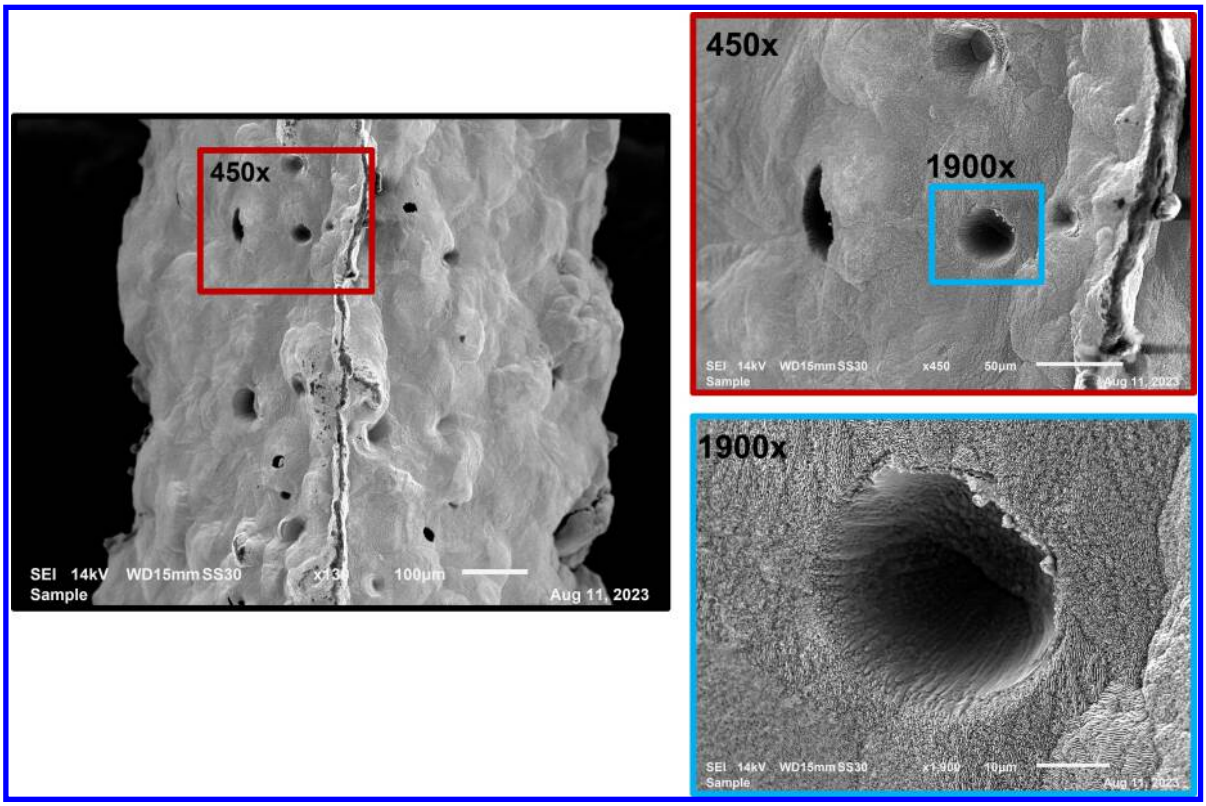

Fig. 9 Voids from the additive manufacturing process that appeared after 12 hours of sputtering erosion. These features may aid in the geometric trapping of sputterants, and the overall self-healing nature of VCMs.

IV. VCM Arcing Behavior

The following section is dedicated to characterizing the arcing response of VCMs compared to traditional MPD and arcjet cathodes, which are typically made of monolithic, or hollow, bulk materials like tungsten and carbon. The volumetric nature of VCMs yields unique electrostatic and thermal properties that give rise to complex arcing physics interactions. A mixture of complementary experimental and computational approaches are taken to examine these phenomena.

We recently investigated the high-power arcing behavior of VCMs in the Large Plasma Device (LAPD) at UCLA by comparing the response of flat and VCM tungsten samples under extreme plasma conditions [17, 19, 26, 27]. Samples of each were placed in a magnetized, pulsed plasma column, and electrically biased to −600 V. This led to the onset of arc discharges, characterized by the runaway release of electrons via thermo-field emission and the attachment of a

high-power density arc, on the order of $GW\ m^{-2}$. The current to both samples during the arcing events was on the order of 50 A, lasting for roughly 20 ms, at a frequency of 0.33 Hz.

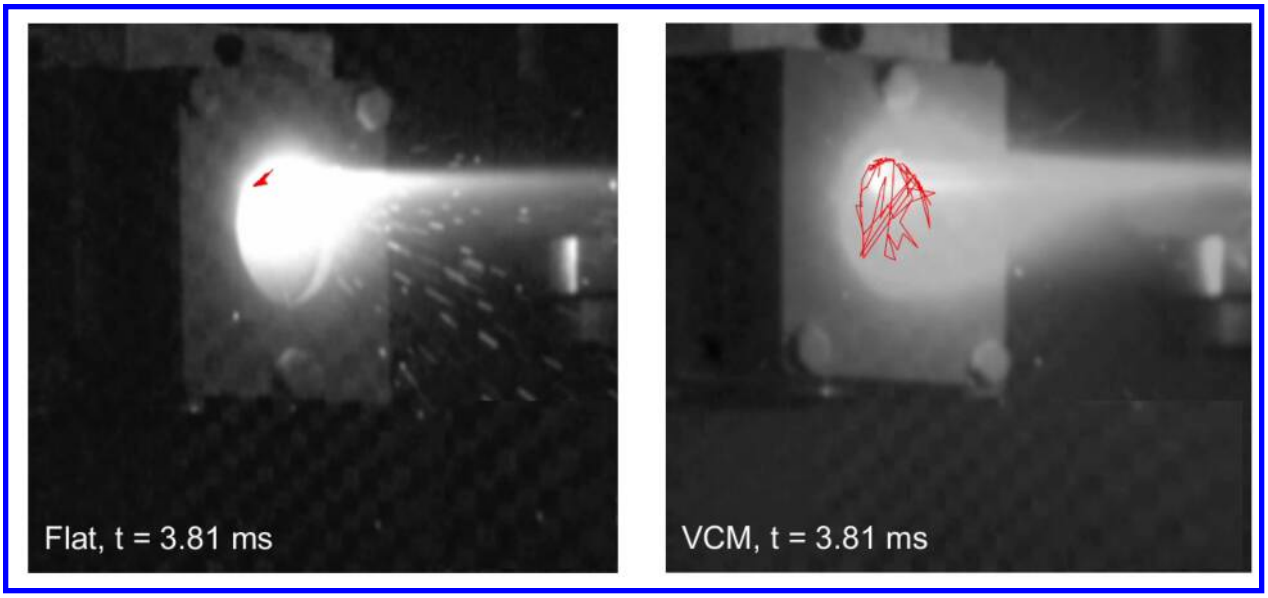

Fig. 10 Differing arcing responses of flat and VCM tungsten samples. A greater quantity of molten ejected material was liberated in the flat sample compared to the VCM. The red traces indicate the motion of the arc path across the samples' face as the arc evolves.

A. Experiment Results

While the electrical characteristics of the two samples were largely the same for each arcing event, high-speed imaging revealed the difference in evaporative erosion between the flat and VCM samples. The arcs that occurred on the flat tungsten remained fixed to one region of the sample, at the triple point junction of vacuum-insulator-tungsten (see red arc traces on Fig. 10). This caused a sustained local heating of a small area, and led to a large quantity of molten ejecta liberated from the surface. By contrast, the arcs on the VCM sample migrated over its surface over time, spreading out the thermal load to a larger area, resulting in less mass ejected compared to the flat sample.

B. Breakdown Simulations

Electrical breakdown simulations provide insight into the behavior of VCMs in an arcing environment. Shown in Fig. 11, the 2D electric fields are computed for a sample of flat tungsten, as well as a sample with pointed surface features; a analogue for a VCM.

Both are surrounded on their edges by an insulating material (boron nitride), so as to be compared with experimental results presented within this section. Particles are released from the cathode surfaces, and any electrical breakdown is detected by integrating Townsend coefficients along the electric field lines. It is found that the VCM reaches breakdown at a lower electric potential compared to the flat surface, and the area over which arcing is favorable is larger. The lower breakdown voltage - which, in some circumstances can be more efficient, and less damaging for thruster operation [15, 28–31] - can be attributed to the field enhancement that occurs at the peaks of the surface features of the VCM. This allows electrons to more easily become liberated from the cathode surface to sustain the arc; this process is then accomplished at lower steady-state cathode temperature, reducing ablative erosion. A similar effect has recently been published for field enhancement of carbon velvet electrodes [32]. The flat sample maintains arcing at the triple point of the insulator, vacuum, and tungsten, whereas the VCM allows for the arc to travel closer to the center of the sample [33]. By encouraging the arc to spread out during operation, this allows for a dispersing of the thermal loads and a potential for less evaporative erosion.

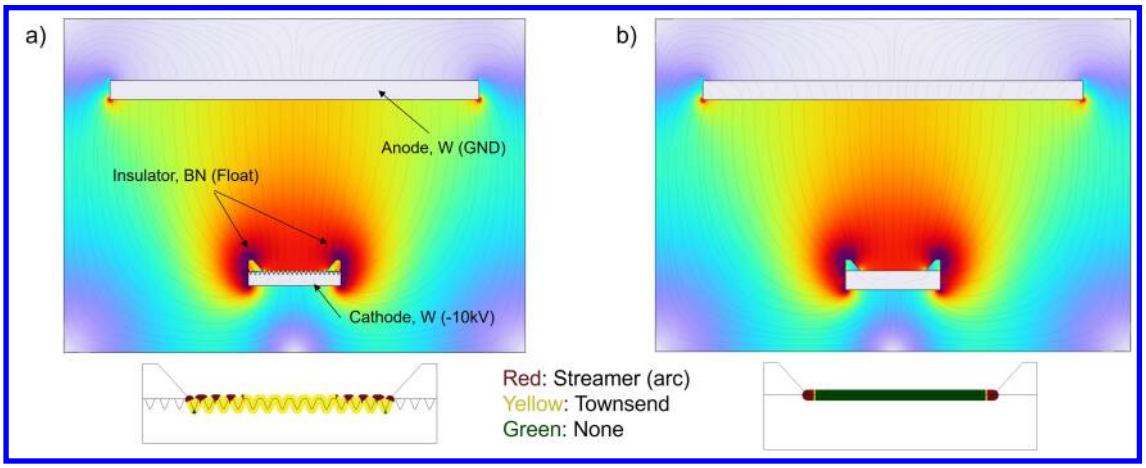

Fig. 11 Breakdown simulation indicating the electric field lines for a) VCM and b) flat samples. VCMs' pointed features lead to enhanced field emission, causing breakdown at a lower potential, relative to flat surfaces. The bottom figures indicate that for arcs on VCMs are more likely to occur at locations other than the triple point junction, leading to the spreading out of the electrical and thermal loads across the face of the sample.

C. Discussion

Taking these experimental and computational results together, it can be concluded that the volumetric, reticulated structure of the VCM appears to improve the absorption of the arcing energy, while still matching the performance of the solid tungsten sample. Future work includes expanding the multi-physics capability of the computational model to include thermal, mechanical, and arc discharge effects, on transient time scales. Additionally, future experiments will further probe the implications of plasma infusion on VCMs, and the consequent effects this has on arcing physics.

V. Summary and Conclusions

We have found that plasma infusion allows for volumetric current carrying, enhancing the ability of VCMs to process high-current space electric propulsion applications. Additionally, the unique VCM architecture creates a favorable environment for sputtering and ablative erosion, which has been demonstrated experimentally in this study. While additive manufacturing (AM) presents a promising method for constructing VCMs with optimized structures for increased current capacity and erosion resistance, it's imperative to carefully consider and mitigate potential drawbacks introduced by AM-specific artefacts. Our future experimental and computational efforts will continue to advance the understanding of longevity and performance of VCMs as high-power electrodes for applications from EP to fusion energy. Overall, the results presented herein highlight the potential of VCMs as a transformative solution for thrust densification in electric propulsion systems, paving the way for more efficient and robust space exploration technologies.

Acknowledgments

This work was supported by the DOE Award DE-AR0001378, "Advanced Materials for Plasma Exposed Robust Electrodes (AMPERE)".

References

[1] Jahn, R., "Physics of Electric Propulsion." 1968.

[2] DONALDSON, A., and Kristiansen, M., "An assessment of erosion resistant cathode materials with potential application in high power electric propulsion devices," *25th Joint Propulsion Conference*, 1989, p. 2515.

[3] MANKINS, J., HARRIS, W., O'HAIR, E., HATFIELD, L., and Kristiansen, M., "Comparison of erosion of various cathode materials in a 30 kWe classarcjet," *28th Joint Propulsion Conference and Exhibit*, 1992, p. 3839.

[4] Pivirotto, T. J., and Deininger, W. D., "Electrode erosion in steady-state electric propulsion engines," *DGLR, DGLR (AIAA) JSASS 20th International Electric Propulsion Conference: Proceedings*, 1988.

[5] Mantenieks, M. A., and Myers, R. M., "100-kW class applied-field thruster component wear," *AIP Conference Proceedings*, Vol. 271, American Institute of Physics, 1993, pp. 1317–1325.

[6] Curran, F. M., Haag, T. W., and Raquet, J. F., "Arcjet cathode phenomena," *JANNAF Propulsion Meeting*, 1989.

[7] Kaminsky, M., *Atomic and ionic impact phenomena on metal surfaces*, Vol. 25, Springer Science & Business Media, 2013.

[8] Behrisch, R., and Eckstein, W., *Sputtering by particle bombardment*, Vol. 1, Springer-Verlag New York, 1981.

[9] Matsunami, N., Yamamura, Y., Itikawa, Y., Itoh, N., Kazumata, Y., Miyagawa, S., Morita, K., Shimizu, R., and Tawara, H., "Energy dependence of the ion-induced sputtering yields of monatomic solids," *Atomic Data and Nuclear Data Tables*, Vol. 31, No. 1, 1984, pp. 1–80. https://doi.org/https://doi.org/10.1016/0092-640X(84)90016-0, URL https://www.sciencedirect.com/science/article/pii/0092640X84900160.

[10] Tartz, M., Heyn, T., Bundesmann, C., Zimmermann, C., and Neumann, H., "Sputter yields of Mo, Ti, W, Al, Ag under xenon ion incidence," *The European Physical Journal D*, Vol. 61, No. 3, 2011, pp. 587–592.

[11] He, Z., Miao, L., Zhu, Z., Liang, F., Song, J., Wang, N., and Hou, X., "Analysis of Sputtering Yield Measurements for Ion Thruster Grid Materials," *AIAA Journal*, Vol. 61, No. 7, 2023, pp. 2799–2809.

[12] Harris III, W. J., *A study of cathode erosion in high power arcjets*, Texas Tech University, 2002.

[13] Harris, W., O'Hair, E., Hatfield, L., and Kristiansen, M., "Cathode erosion research on medium to high power arcjet thrusters," *IEEE Transactions on Electron Devices*, Vol. 28, 1993, pp. 280–292.

[14] Peng, W., Yibai, W., Yong, L., Baojun, W., Zhang, K., Haibin, T., and Jinbin, C., "Cathode erosion site distributions in an applied-field magnetoplasmadynamic thruster," *Plasma Science and Technology*, Vol. 22, No. 9, 2020, p. 094008.

[15] Polk, J., Kelly, A., Jahn, R., KURTZ, H., and AUWETER-KURTZ, M., "Mechanisms of hot cathode erosion in plasma thrusters," *21st International Electric Propulsion Conference*, 1990, p. 2673.

[16] Li, G. Z., and Wirz, R. E., "Persistent sputtering yield reduction in plasma-infused foams," *Physical Review Letters*, Vol. 126, No. 3, 2021, p. 035001.

[17] Sabiston, G., and Wirz, R. E., "Sputtering Reduction Optimization via Volumetrically Complex Materials," *Bulletin of the American Physical Society*, 2022.

[18] Sabiston, G., and Wirz, R. E., "Optimization of Additively Manufactured Plasma-facing Surfaces with Consideration of Plasma Infusion Effects," *Bulletin of the American Physical Society*, 2023.

[19] Wirz, R. E., Wan, G., Sabiston, G., Konopliv, M., Thuppul, A., et al., "Persistent Sputtering Yield Reduction in Plasma-Infused Materials for Plasma Propulsion and Fusion," *Bulletin of the American Physical Society*, 2022.

[20] Huerta, C. E., and Wirz, R. E., "Ion-induced electron emission reduction via complex surface trapping," *AIP advances*, Vol. 9, No. 12, 2019, p. 125009.

[21] Huerta, C., Matlock, T., and Wirz, R., "View factor modeling of sputter-deposition on micron-scale-architectured surfaces exposed to plasma," *Journal of Applied Physics*, Vol. 119, No. 11, 2016, p. 113303.

[22] Patino, M., Raitses, Y., and Wirz, R., "Electron emission from nano and microstructured materials for plasma applications," *APS Annual Gaseous Electronics Meeting Abstracts*, 2016, pp. QR2–003.

[23] Ottaviano, A., Thuppul, A., Hayes, J., Dodson, C., Li, G. Z., Chen, Z., and Wirz, R. E., "In situ microscopy for plasma erosion of complex surfaces," *Review of Scientific Instruments*, Vol. 92, No. 7, 2021.

[24] Nakano, T., and Baba, S., "Gas pressure effects on thickness uniformity and circumvented deposition during sputter deposition process," *Vacuum*, Vol. 80, No. 7, 2006, pp. 647–649.

[25] Emmoth, B., and Bergsaker, H., "Sticking of sputtered particles to different surfaces," *Nuclear Instruments and Methods in Physics Research Section B: Beam Interactions with Materials and Atoms*, Vol. 33, No. 1-4, 1988, pp. 435–437.

[26] Ottaviano, A., "Plasma Interactions and Electron Dynamics for Volumetrically Complex Materials," Ph.D. thesis, University of California, Los Angeles, 2023.

[27] Ottaviano, A., Konopliv, M., Collins, A., Sabiston, G., Wan, G., Vincena, S., Look, T., Travis, P., Gonzalez, J., Pribyl, P., Carter, T., and Wirz, R., "Electron Emission and Arc Behavior of Plasma-Robust Volumetrically Complex Materials," *Bulletin of the American Physical Society*, 2022.

[28] Jeffers, B., "Cathode Erosion and Propellant Injection System of a Low-Voltage, Liquid-Fed Pulsed Plasma Thruster," Ph.D. thesis, Purdue University, 2023.

[29] CHAMBERLAIN, F., KELLY, A., and JAHN, R., "Electropositive surface layer MPD thruster cathodes," *25th Joint Propulsion Conference*, 1967, p. 2706.

[30] Fillmore, J. S., von Jaskowsky, W., Kelly, A., and Jahn, R., "An experimental study of lithium dispenser cathodes in the MPD thruster," Master's thesis, Princeton University, 1998.

[31] Codron, D., Goodfellow, K. D., Downey, R. T., and Erwin, D. A., "Solid thoriated tungsten cathode arc discharges for electrically propelled spacecraft," *IEEE Transactions on Plasma Science*, Vol. 40, No. 7, 2012, pp. 1926–1932.

[32] Xie, L. N. Z. Q. e. a., H., "A stable atmospheric-pressure plasma for extreme-temperature synthesis," *Nature*, Vol. 623, No. 7989, 2023, pp. 964–971.

[33] Damamme, G., and Le Gressus, C., "Simulation of the triple junction effects in vacuum devices," *Proceedings of Conference on Electrical Insulation and Dielectric Phenomena-CEIDP'96*, Vol. 2, IEEE, 1996, pp. 562–566.